

DNA-templated self-assembly of bradykinin into bioactive nanofibrils

Article

Accepted Version

Lourenço, T. C., de Mello, L. R. ORCID: <https://orcid.org/0000-0001-7630-5087>, Icimoto, M. Y. ORCID: <https://orcid.org/0000-0002-0746-5279>, Bicev, R. N. ORCID: <https://orcid.org/0000-0002-5951-9005>, Hamley, I. W. ORCID: <https://orcid.org/0000-0002-4549-0926>, Castelletto, V., Nakaie, C. R. ORCID: <https://orcid.org/0000-0001-7057-1990> and da Silva, E. R. ORCID: <https://orcid.org/0000-0001-5876-2276> (2023) DNA-templated self-assembly of bradykinin into bioactive nanofibrils. *Soft Matter*, 19 (26). pp. 4869-4879. ISSN 1744-6848 doi: <https://doi.org/10.1039/d3sm00431g> Available at <https://centaur.reading.ac.uk/112395/>

It is advisable to refer to the publisher's version if you intend to cite from the work. See [Guidance on citing](#).

To link to this article DOI: <http://dx.doi.org/10.1039/d3sm00431g>

Publisher: Royal Society of Chemistry (RSC)

All outputs in CentAUR are protected by Intellectual Property Rights law, including copyright law. Copyright and IPR is retained by the creators or other copyright holders. Terms and conditions for use of this material are defined in the [End User Agreement](#).

www.reading.ac.uk/centaur

CentAUR

Central Archive at the University of Reading

Reading's research outputs online

DNA-Templated Self-Assembly of Bradykinin into Bioactive Nanofibrils

Thiago C. Lourenço¹, Lucas R. de Mello¹, Marcelo Y. Icimoto¹, Renata N. Bicev¹, Ian W. Hamley², Valeria Castelletto², Clovis R. Nakaie¹, Emerson R. da Silva^{1,*}

¹ Departamento de Biofísica, Universidade Federal de São Paulo, São Paulo 04062-000, Brazil

² Department of Chemistry, University of Reading, Reading RG6 6AD, United Kingdom

ABSTRACT

Bradykinin (BK) is a peptide hormone that plays a crucial role in blood pressure control, regulates inflammation in the human body, and has recently been implicated in the pathophysiology of COVID-19. In this study, we report a strategy for fabricating highly ordered 1D nanostructures of BK using DNA fragments as a template for self-assembly. We have combined synchrotron small-angle X-ray scattering and high-resolution microscopy to provide insights into the nanoscale structure of BK-DNA complexes, unveiling the formation of ordered nanofibrils. Fluorescence assays hint that BK is more efficient at displacing minor-groove binders in comparison with base-intercalant dyes, thus, suggesting that interaction with DNA strands is mediated by electrostatic attraction between cationic groups at BK and the high negative electron density of minor-grooves. Our data also revealed an intriguing finding that BK-DNA complexes can induce a limited uptake of nucleotides by HEK-293t cells, which is a feature that has not been previously reported for BK. Moreover, we observed that the complexes retained the native bioactivity of BK, including the ability to modulate Ca²⁺ response into endothelial HUVEC cells. Overall, the findings presented here demonstrate a promising strategy for the fabrication of fibrillar structures of BK using DNA as a template, which keep bioactivity features of the native peptide and may have implications in the development of nanotherapeutics for hypertension and related disorders.

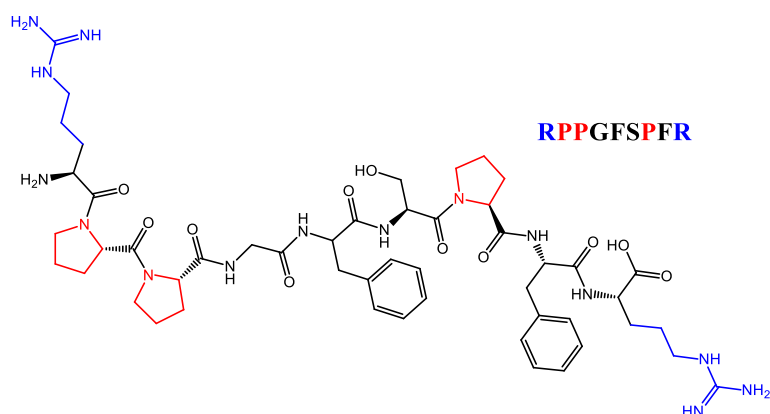
*Corresponding author: er.silva@unifesp.br

INTRODUCTION:

Bradykinin (BK) is a potent bioactive peptide, belonging to the kinin protein group, and exhibiting strong agonistic activity for the B2 receptor of GPCR proteins.^{1,2} Its discovery more than 70 years ago³ marked a milestone in medical research, as scientists soon realized its ability to modulate intracellular calcium levels, control blood pressure, produce a vasodilator effect, and play a significant role as a pro-inflammatory mediator.⁴⁻⁶ This remarkable peptide hormone continues to surprise the research community, and recently, it has been proposed to play a pivotal role in the pathophysiology of SARS-CoV-2.^{7,8} According to studies conducted during the COVID-19 pandemic, the downregulation of the expression of the angiotensin-converting enzyme 2 (ACE2) inhibits degradation of both BK and its analog des-Arg⁹-BK, promoting a “bradykinin storm” that increases vascular permeability and exacerbates the severity of disease symptoms.^{9,10}

Although the pharmacological mechanisms of BK and its analogs are relatively well understood for decades,^{1,2} their use in the development of nanostructured materials is not widely reported in the literature. While a few recent reports demonstrate hybrid systems involving the conjugation of BK with polymeric chains¹¹ and the folding of 2D nanoparticles on solid substrates,¹² studies demonstrating BK-based nanostructured assemblies are still lacking. Nanostructured materials offer significant advantages in the production of therapeutic vehicles as they can act as carriers for active molecules or facilitate a pre-concentration effect that enhances the therapeutic potential of bioactive building blocks.¹³⁻¹⁷ The utilization of this approach has found particular application in the field of DNA-based therapeutics delivery. In recent years, there has been a growing interest in employing biopolymers as a promising strategy for the development of such architectures.¹⁸⁻²⁰ This is particularly relevant for 1D assemblies, which have one dimension much larger than the others and display a greater capacity for unique biological interactions. These structures can align and form entangled networks that can serve as scaffolds, mimicking the extracellular matrix and possibly offering enhanced suitability for applications in biotechnology.^{21,22} We hypothesize that the scarcity of nanostructures based on BK may be related

to features of the primary structure, which is characterized by a nonameric amino acid sequence, RPPGFSPFR (Scheme 1). The abundance of prolines in the BK composition, representing one-third of the sequence, leads to a kinked arrangement that makes twisting and folding energetically costly. These structural characteristics may pose a significant challenge in producing regular nanostructures.



Scheme 1. Chemical structure of the bradykinin peptide. Sidechains of proline residues responsible for conveying rigidity to the strand are highlighted in red. Arginine sidechains, bearing cationic charges under physiological conditions, are marked in blue.

To overcome this challenge, we investigate here the use of DNA strands as a mediator that assists in self-assembly to induce the formation of supramolecular structures via electrostatic interaction and provide directionality to stimulate the formation of regular arrangements with one-dimensional symmetry.^{23–25} The amphiphilic design of BK, with arginine residues at both ends and hydrophobic residues in the central portion, makes it an ideal candidate for the production of self-organized arrangements based on arginine,²⁶ a cationic amino acid highly hydrophilic and able to interact easily with DNA via electrostatic attraction.^{27,28} We found that while bradykinin itself exhibits low self-assembling capabilities, in the presence of DNA strands it can form nanofibrils. Fluorescence assays revealed that BK-DNA binding primarily occurs via minor-groove interactions, making it a useful feature for templating the formation of fibrillar structures. We also investigated the ability of the BK-DNA complexes to promote intracellular uptake of DNA fragments and found that BK assists the entry of DNA in the cytosol of HEK-293t cells. In

addition, the BK-DNA complexes have been found to modulate Ca^{2+} response into endothelial HUVEC cells, demonstrating that the native bioactivity of BK is preserved upon complexation with nucleic acids. Overall, the findings presented here suggest a promising strategy to fabricate self-organized, fibrillar nanoassemblies made from BK, which potentially have applications in nanotherapeutics, especially for blood pressure control and related diseases.

MATERIALS AND METHODS

Bradykinin synthesis and DNA fragmentation: the bradykinin peptide, with amino acid sequence $\text{NH}_2\text{-RPPGFSPFR-COOH}$, was purchased from AminoTech (Sao Paulo, Brazil). According to the manufacturer, they were synthesized manually using standard solid-phase peptide synthesis with the Fmoc strategy and Wang resin. Peptides were purified through semi-preparative liquid chromatography (LC) procedures using either solvent A (H_2O with 0.1% TFA) or solvent B (90% MeCN in H_2O with 0.1% TFA). A linear gradient was applied at a flow rate of 10 mL/min, and the detection of peaks was carried out at 220 nm. The synthesis yielded the product in the form of TFA salt which were been characterized by liquid chromatography coupled to mass spectroscopy (LC-MS), indicating purity levels above 99% (Supporting Information file, SI, Figure S1). The molecular weight is $M_w = 1060.7$ (calculated $M_w = 1060.3$). All reagents used in the synthesis had HPLC purity levels and were acquired from Merck (Sigma-Aldrich). Herein, we have used calf-thymus DNA as a model for the nucleic acid component in our study. The reasons for this choice rely on the widespread use of calf-thymus DNA in binding assays,²⁹ its suitability as a physicochemical model demonstrated in previous studies,^{24,27,30} and on the affordability of these materials. The DNA ($M_w = 660$ g/mol per base pair) was obtained from Sigma-Aldrich (D1501) and fragmented by sonication into smaller pieces with an average length of approximately 150 base pairs, as confirmed by electrophoresis runs (SI file, Figure S2). The fragmentation was achieved using ultrasonication with a Diagenode Bioruptor, following the procedure described elsewhere.³¹ DNA fragments were stained with YOYO-1 dye to serve as a reporter in fluorescence imaging assays. The concentration of fresh DNA stocks was determined

by measuring absorbance at 260 nm and considering an average extinction coefficient of $\epsilon_{260} = 13200 \text{ M}^{-1}\cdot\text{cm}^{-1}$. The A260/A280 ratios were over 1.8, indicating appropriate levels of purity.

Fluorescence Spectroscopy: steady-state fluorimetry assays were conducted using a Shimadzu F-2500 fluorimeter to analyze the emission behavior of peptide and peptide/DNA solutions prepared with various fluorophores. The dyes employed in this study included 1-anilino-8-naphthalene sulfonate (ANS), thioflavin T (ThT), ethidium bromide (EtBr) from Sigma-Aldrich, and the cyanine dye SyBr Safe from ThermoFisher. The concentrations of fluorophore used in the preparations were as follows: ANS at 70 μM , ThT at 31 μM , EtBr at 25 μM , and SyBr at 20 μM . The choice of these concentration values was based on previous literature and recommendations from manufactures.^{30,32} To determine the critical aggregation concentrations of peptides, we prepared a series of peptide solutions in ultrapure water with concentrations ranging from 17 μM to 9 mM, in the presence of ANS as a fluorescent probe. We selected this concentration range because it covers the critical concentration values commonly observed for short peptides that share physicochemical similarities with BK.^{24,26,33} In addition, we conducted experiments with BK-DNA complexes in the presence of other fluorophores, keeping the DNA concentration constant at 60 μM and titrating BK. Intensities have been normalized to the emission of the DNA solution (without peptide) and the fluorescence of the solution containing only the fluorophore was taken as the background threshold. The experiments were carried out in independent duplicates at room temperature using quartz cuvettes with a 10 cm path length.

Transmission Electron Microscopy (TEM): Transmission electron microscopy (TEM) imaging was conducted using a JEOL 2100 FEG-TEM microscope. To enhance particle adhesion, the grids for TEM samples were subjected to plasma glow discharge treatment. Aliquots of 3 μl were extracted from 9 mM peptide solutions and deposited onto 300-mesh lacey carbon grids, which were then negatively stained using a 2% uranyl acetate solution. The microscope operated at an acceleration voltage of 200 keV, and data analysis was performed using Image J software.³⁴

Atomic Force Microscopy (AFM): AFM imaging was conducted using a Park NX10 instrument operating in dynamic mode, which is better suited for soft materials. To prepare the samples, droplets from 9 mM BK solutions were deposited onto freshly cleaved mica substrates. For

BK/DNA complexes, samples were prepared from solutions containing peptide and nucleic acids at a 6:1 molar ratio. After casting, substrates were allowed to rest for approximately 10 minutes, and excess solution was removed using a paper filter. The samples were left to dry overnight in a desiccator. Images were captured at a resolution of 512×512 pixels with a scanning frequency of 0.5 Hz. Image enhancements and processing were performed using Gwyddion software.³⁵

Small-Angle X-ray Scattering (SAXS): Small-angle X-ray scattering (SAXS) data were acquired at beamline B21 of the Diamond Light Source (Didcot, UK). The peptide solutions, with a concentration of 9 mM, were injected into a quartz capillary with a diameter of 1.8 mm using a BioSAXS device, in a vacuum chamber. The SAXS beamline was operated with an X-ray energy of 12.4 keV, covering a q -range between 0.1 and 10 nm^{-1} . A PILATUS 2 M detector recorded the scattering patterns, and ten frames per sample were collected, which were averaged, and background subtracted in the absence of radiation damage. Data fitting was carried out using the SASfit program.³⁶

Cell culture and confocal microscopy: HEK-293t cells were maintained in DMEM supplemented with 10% fetal bovine serum and 2 mM glutamine, and incubated at $37 \text{ }^\circ\text{C}$ in a humidified atmosphere containing 5% CO_2 . Glass coverslips were carefully placed in a 24-well plate and seeded with 50,000 cells, which were allowed to grow for 24 hours. Nanocomplexes were prepared by mixing 5 μg of labeled DNA fragments with the appropriate amount of peptide stock to achieve a 2:1 molar ratio in 50 μl of ultrapure water. Since DNA carries two negative charges per base pair and BK possesses two positive charges per strand, this molar ratio also generates a 2:1 charge ratio and creates an excess of positive charge. This surplus promotes the interaction with cell membranes while minimizing potential cytotoxicity effects that may arise from cationicity.^{24,30} The mixtures were then incubated at $37 \text{ }^\circ\text{C}$ for 30 minutes and transferred to 950 μl of DMEM. The nanocomplexes were incubated with cells for 4 hours, while a negative control was prepared by incubating only DNA under the same conditions. After incubation, the samples were washed 3 times with PBS to remove unbound cells and complexes. The cells were then fixed with 4% paraformaldehyde and nuclear staining was carried out with DAPI (Invitrogen, California) in PBS for 5 minutes at room temperature. Confocal microscopy was performed using a Leica TCS SP8 microscope with appropriate laser sources for excitation

wavelengths of each fluorophore. ImageJ software was used for image processing. **Calcium Influx Assay:** HuVEC cells were cultured in RPMI medium supplemented with 10% FBS (Vitrocell, Campinas, São Paulo, Brazil). In the following, they were seeded at 20,000 cells per well, and incubated for 24 hours to adhere and grow. After this period, the media was replaced with a solution containing Fluo-4M (ThermoFisher) at a concentration of 10 μ M in DMSO. The cells were kept in the dark in the presence of Fluo-4M for 2 hours, and then washed with a DBSS buffer to remove excess dye. The cultures were then incubated with BK (or with BK-DNA complexes) at concentrations of 1 μ M peptide and the changes in the intracellular calcium levels were monitored by measuring the fluorescence of Fluo-4 AM using a spectrofluorometer plate reader Flexstation 3 (Molecular devices). Fluorescence was monitored for about 2 minutes yielding the kinetics of the Ca^{2+} response.

RESULTS AND DISCUSSIONS

Fluorimetry assays: BK-DNA interaction

We first characterized the aggregation behavior of BK by fluorescence to semiquantitatively estimate critical aggregation concentration (C.A.C.) values. This procedure is widely used in the study of peptide self-assembly,^{16,17,24,26,33} and by estimating C.A.C. values of BK solutions in the presence or absence of DNA, we can compare the aggregation behavior of the peptide and gain insights into the role of DNA as a mediator of aggregation. These assays were performed by preparing samples with different peptide concentrations in solutions containing ANS, a fluorescent probe whose emission profile is highly sensitive to the polarity of the medium.^{30,37} When peptide aggregates are formed in an aqueous medium, the ANS molecule tends to be lodged inside these clusters and the change in hydrophobicity of the chemical microenvironment leads to a significant increase in fluorescence and a hypsochromic effect with the peak emission shifting towards blue.³⁷ Figure 1A displays the results of one fluorescence series where it is possible to observe that the ANS emission intensity exhibits low growth in the presence of the peptide in solution, presenting moderate growth when the BK concentration exceeds values of the order of 1.2 mM (Figure 1A). Similarly, visualization of ANS-containing

solutions and different concentrations of BK under ultraviolet illumination, Figure 1B, reveals that the samples are characterized by a greenish-yellow glow even at high peptide concentrations, resulting from the emission of the fluorophore in the range 505-515 nm (see SI file, Figure S3A). In contrast, the fluorescence behavior as a function of peptide concentration is completely different when DNA fragments are present in solution. In this case, it is observed that the emission intensity increases substantially from $\sim 190 \mu\text{M}$, about an order of magnitude below the critical point observed when bradykinin is alone in solution (Figure 1A, black squares). Furthermore, visual inspection of BK/DNA solutions under ultraviolet light ($\lambda = 400 \text{ nm}$) shows that the fluorescence appearance changes completely, highlighting an intense turquoise-blue glow at high peptide concentrations, attesting to the hypsochromic effect indicative of aggregate formation in solution (see SI file, Figure S3C).^{30,37} Therefore, the above findings constitute a first indication of nucleic acid complexation with BK, revealing that DNA fragments act as inducers of peptide aggregation in aqueous media.

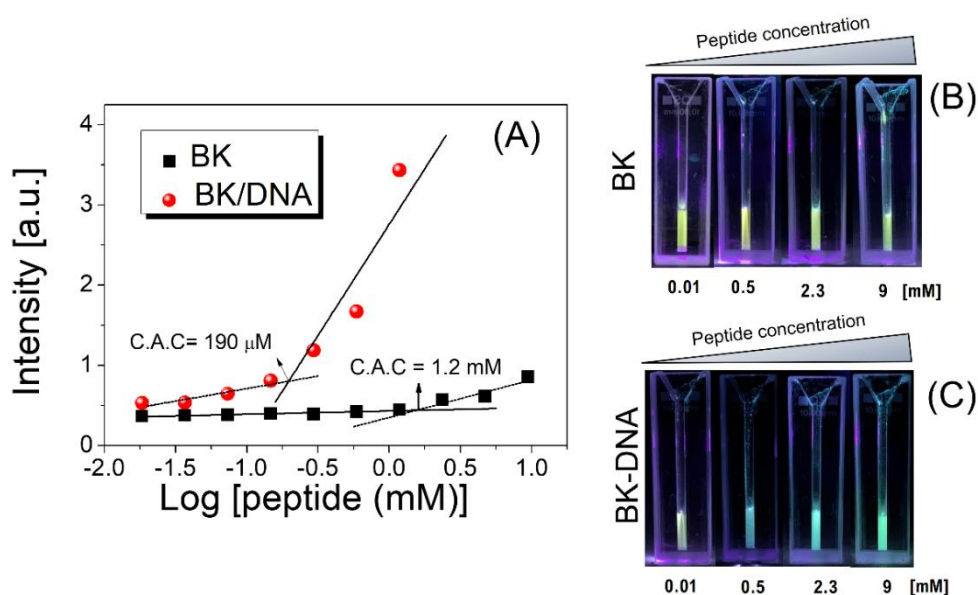


Figure 1: (A) Fluorescence intensity of the dye ANS in the presence of different BK concentrations. Black squares correspond to solutions containing only BK, whereas red circles correspond to samples also containing $60 \mu\text{M}$ DNA. (B) and (C) Photographs from solutions containing peptides at the indicated concentrations under illumination with UV light (400 nm).

To further elucidate the interaction between BK and DNA, we carried out dye displacement assays using fluorescent probes. Specifically, we employed ethidium bromide (EtBr), a base-intercalating agent,^{32,38} and SYBR safe, a minor-groove binder,³⁹ to investigate the preferred binding regions of BK to DNA. The assays were performed in solutions containing 60 μM DNA complexed with the corresponding fluorophore, followed by titration with BK aliquots. As anticipated, the addition of peptides to the solutions caused a discernible decrease in fluorescence intensity due to the displacement of the dyes by BK binding to DNA strands. Fluorescence intensity plots as a function of BK concentration (Figures 2A and B) revealed that BK was more effective at displacing SYBR safe than EtBr. In Figure 2C, a comparison of the BK concentrations required to displace 50% of the dye revealed an $\text{EC}_{50} = 7.9 \pm 2.6 \mu\text{M}$ for SYBR safe and $\text{EC}_{50} = 14.3 \pm 1.7 \mu\text{M}$ for EtBr. The unpaired t-Student test of the EC_{50} values above yields a significance level of approximately 90%, suggesting that BK is more likely to displace SyBr than the base-intercalating dye EtBr. The presented results indicate that BK is more efficient in displacing SyBr molecules from DNA duplexes compared to EtBr, as it requires a lower average concentration to achieve the EC_{50} . Since SyBr is known for its binding to the minor groove of DNA,³⁹ BK efficiently competes for these binding sites on the DNA duplexes. Given that the minor grooves possess the highest electron density across the entire DNA strand,⁴⁰ we hypothesize that the electrostatic attraction between the phosphate sites on DNA and the cationic groups in the arginine sidechains of BK is likely a significant driving force in the formation of these complexes. This hypothesis is further supported by additional dye displacement assays conducted with the des-Arg9-BK analogue (referring to the bradykinin sequence with the arginine amino acid removed at position 9), which results in a lower cationic charge compared to native BK.⁴¹ These assays, depicted in Figure S4, demonstrate that this less cationic analog exhibits a higher efficacy in displacing EtBr rather than SyBr, emphasizing the significance of electrostatic attraction in the formation of BK-DNA complexes. In addition, dye displacement assays performed with methyl green, a major-groove binder,⁴² indicated that the peptide is not capable of shifting the dye suggesting that this region is not substantially involved in the binding of BK to DNA (SI file, Figure S5). These findings suggest that electrostatic interactions play a

predominant role in the BK-DNA interaction, particularly when considering that the minor-groove region has the highest (anionic) electronic density in the DNA double helix.⁴³

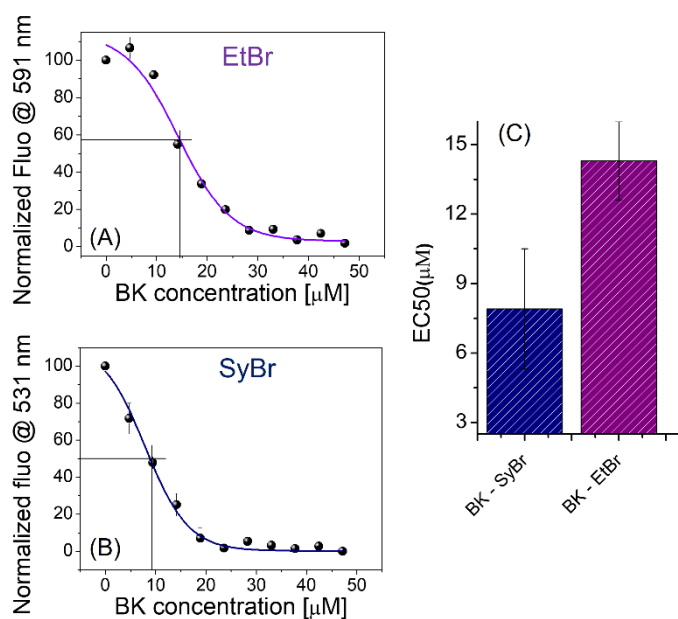


Figure 2: Dye displacement assays on BK titration series in 60 μM DNA complexed with the base-intercalating agent, EtBr (A), and the cyanine minor-groove binder, SyBr safe (B). The data are presented as the mean \pm SD of independent duplicates, and the solid lines correspond to sigmoidal fits. (C) Comparison of the EC50 values found in the titration series.

Nanoscale structure:

To extract detailed information about the nanoscale structure of the BK peptide and its complex with DNA, we have performed a set of experiments combining small-angle X-ray scattering (SAXS) and electron and atomic force microscopies (TEM and AFM). While microscopy methods have the advantage of providing direct space visualizations that allow for the discrimination of aggregate morphology, SAXS provides structural information in solution, under native conditions that avoid artifacts arising from drying and sample preparation.^{44,45} In Figure 3A, SAXS curves from aqueous samples containing BK, DNA, or BK/DNA complexes exhibit very distinct scattering profiles, indicating that the nanoscale morphology of aggregates in the solutions is strongly affected by complexation.

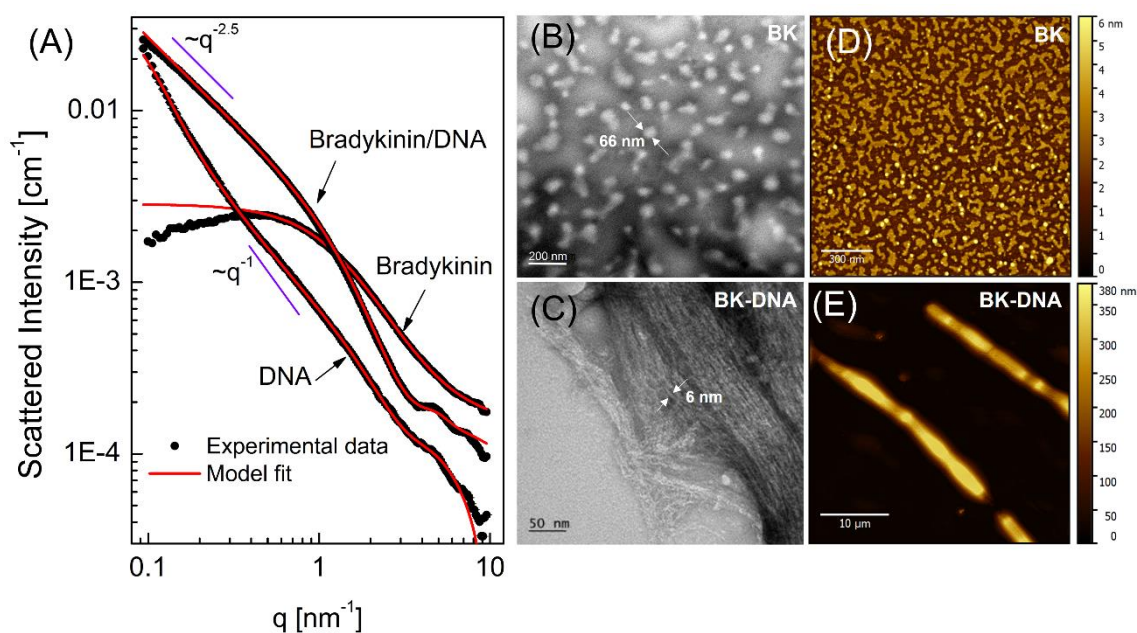


Figure 3. Nanoscale structural data. (A) SAXS curves from aqueous solutions containing BK, DNA, or BK-DNA complexes. The red lines are model fits described in the text. (B) Electron microscopy images showing negative-stained BK aggregates and (C) BK-DNA fibrils. (D) and (E) AFM topography images from BK and BK-DNA solutions, respectively, dried on mica substrates.

In the case of scattering data from BK solutions, the low- q region is characterized by a smooth plateau with a moderate descent near $q = 0$. The intermediate-to-high q -range features a steep decay scaling with $\sim q^{-1}$, which is consistent with the scattering pattern of chains in solution.^{46,47} Quantitative analysis of these data was performed by fitting a Gaussian coil form factor plus a flat background to the scattering profile (see SI file for detail, Eqs. S1 and S2),^{47,48} which revealed fitting parameters: radius of gyration $R_g = 1.2$ nm and a Flory exponent $\nu = 0.51$, indicating with BK strands with a disordered conformation in a theta-solvent condition.^{46,49} The reduction of the scattering observed near to $q = 0$ can be interpreted as a consequence of the repulsion between peptide strands, likely arising from electrostatic repulsion between charged chains. Therefore, the SAXS data provide evidence that bradykinin in aqueous medium does not self-organize into supramolecular arrangements with long-range order, even at concentrations as high as 9 mM. The best fitting parameters emerging from full-range SAXS data fits are summarized in Table 1.

Table 1. Model fitting parameters arising from SAXS data analysis.

System	Form factor model	Structural parameters
BK	Gaussian coil	$R_g = 1.2$ nm, $\nu = 0.5$
DNA	Porod cylinder	$R = 1.0$ nm
BK-DNA	Cylindrical shell	$R_c = 1.0$ nm, $\Delta R = 1.3$ nm

In contrast, SAXS profiles obtained from BK-DNA complex samples exhibit in the low-angle region a decay according to a power-law with $\sim q^{-2.5}$, characteristic of interconnected fibrillar networks with mass fractal topology features.^{49,50} The scattering profile of these samples is significantly distinct from that obtained from solutions containing only DNA fragments (see Fig. 3A), demonstrating that complexation gives rise to new morphologies with the appearance of polymorphs completely distinct from the biomolecules pre-complexation. SAXS data from DNA samples were satisfactorily fitted with a Porod cylinder form factor (Eq. S3) with a radius of $R = 0.97$ nm, fully consistent with the radius of the DNA double helix (see SI file for details).^{24,40,47}

The fit of the data from BK-DNA complexes was performed with a core-shell cylinder form factor,⁴⁷ Eq. S4, leading to an internal radius of $R_c = 1.0$ nm and shell thickness of $\Delta R = 1.2$ nm. These structural parameters indicate cylindrical particles with diameters of about 4.4 nm, consistent with cores formed by DNA chains wrapped by peptide layers that structure to give rise to fibrils that form a network.^{24,30} The formation of cylindrical core-shell assemblies guided by nucleic acids has been previously observed for other short peptide with amphiphilic characteristics.^{24,25,51} In the case of BK, arginine residues on both ends of the strands likely mediate electrostatic attraction with the anionic phosphate groups of the DNA backbone. Additionally, the bulky primary structure of BK, which includes hydrophobic amino acids, assists self-assembly through the hydrophobic effect. The lateral packing and π - π stacking formed by central phenylalanine side chains of adjacent strands also contributes to directionality and further promotes self-assembly along the long axis of DNA duplex.^{17,24}

Electron microscopy images of dried BK samples revealed the presence of irregular structures, as shown in Figure 3B. The aggregates found have varied sizes, typically of the order of a few tens of nanometers. In this case, we interpret that the drying process during sample preparation may be at the origin of these larger aggregates observed in TEM images. Atomic force microscopy topography data obtained on BK samples dried on mica substrates, Figure 3D, also reveal the presence of irregular aggregates with lateral dimensions on the order of tens of nanometers and heights on the order of a few nanometers. Although larger in lateral sizes, the topography appearance of these aggregates is quite similar to BK nanoaggregates folded on Cu(110) surfaces previously reported in literature.¹² In Figure 3C, electron microscopy images clearly show extensive fibrillar arrangements induced by BK-DNA complexes. Assays performed in the presence of Thioflavin T, a fluorescent probe sensitive to amyloids,^{37,52} indicate a substantial enhancement in the emission yield upon complexation, thus suggesting that the fibrils possess amyloid-like characteristics (SI file, Figure S6). Investigations into the secondary structure of BK and BK-DNA complexes were also conducted using circular dichroism. The results indicate that BK in solution exhibits mixed signature with polyproline II and β -sheet

features, while the presence of a small amount of DNA leads to the appearance of distinct β -sheet signals in the spectra (see SI file, Figure S7). Together with the fibrillar morphology observed in SAXS and microscopy assays, and the thioflavin emission data, these spectroscopic findings provide further evidence for the amyloid-like features present in BK-DNA assemblies.

Despite the relatively short length of the DNA fragments ($\sim 150 \times 0.34 = 51$ nm), the fibrils have lengths reaching the micrometer range. It is worth stressing that the size of the nucleic acid strands used here is roughly equivalent to the persistence length of DNA duplexes,⁵³ which makes the fragments behave as rigid rods that can nucleate self-assembly. This highlights the templating behavior of the DNA fragments, which can induce fibrillization over much longer length scales. TEM images shown in the SI file, Figure S8, depict nanofiber networks spread across larger surfaces. Measurements performed on over 150 fibrils across the samples indicate average diameters of 5.2 ± 2.8 nm, consistent with the structural parameters obtained from SAXS data fitting. Samples from solutions containing high concentrations of BK-DNA (~ 9 mM peptide) were intentionally dried on mica substrates and examined using AFM (Figure 3E). Under these highly concentrated conditions, we observed the formation of larger structures with lengths reaching the micrometer range and diameters in the range of a few hundred nanometers. This observation confirms that the templating effect of DNA strands is capable of influencing self-assembly into one-dimensional (1D) arrangements at length scales significantly larger than the dimensions of the DNA strands.

Putting the findings above together, we observe that both the in-solution information obtained via SAXS and the data on dried samples obtained via TEM and AFM reveal that BK alone has a limited capacity to aggregate into ordered arrangements, whereas complexation with nucleic acids emerges as an effective method for directing the organized aggregation of BK into 1D arrangements. Considering that both BK and DNA are charged molecules, we hypothesize that complexation follows a similar pathway observed in other systems of oppositely charged polyelectrolytes.^{54,55} The representation of the proposed mechanism for which fibers are formed is shown in Figure 4. According to this proposition, the first step for association is the electrostatic

attraction between the cationic groups of BK and the anionic sites of the DNA double helix. From this step onwards, the DNA duplex acts as a nucleation center, facilitating the condensation of peptide chains along its backbone. Additionally, self-association occurs between BK strands through multiple intermolecular interactions, including hydrogen bonding, hydrophobic attraction, and π - π stacking between aromatic side chains (Step 2). These interactions provide directionality for the growth of the fiber along its long axis.^{26,56-59} However, complexation is more intricate than the simple "electrostatic attraction", as thermodynamic factors play a key role in completing the association, particularly involving the release of counterions and the destruction of solvation layers.^{55,60} Prior to complexation, DNA and peptide chains are immersed in the solvent, surrounded by their respective counterions (Na^+ and TFA^- in this case), resulting in an overall electrostatically neutral solution. In addition, these species also possess solvation layers where water molecules appear more structured in comparison with the molecules in bulk solution. Upon the formation of BK/DNA complexes through the association of peptides and nucleic acids, these counterions and water molecules are released into the bulk solution, leading to a significant gain in translational entropy. Although the association between DNA and peptide chains results in a loss of conformational entropy for these biomolecules, the increase in translational entropy of the counterions and solvent molecules previously retained in the solvation layers compensates for this effect, resulting in an overall entropy gain that makes the association thermodynamically stable.^{54,58,59} Finally, the elongation process is consolidated, and fiber ripening takes place, leading to the formation of fibrillar networks (Step 3).

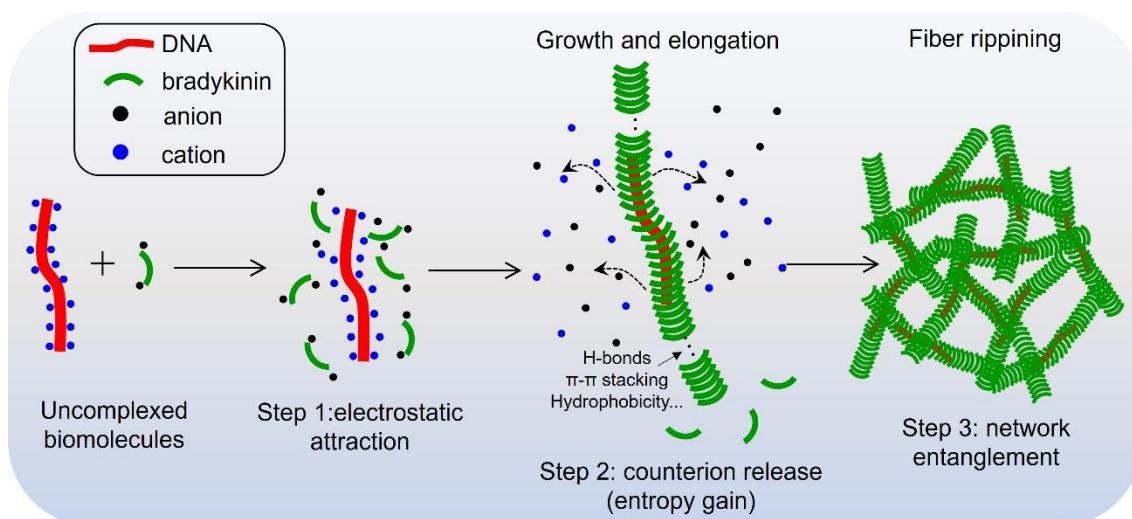


Figure 4. Representation of the proposed pathway for the formation of BK/DNA fibrillar complexes. The process is initiated by electrostatic attraction between oppositely charged species. The release of counterions and water molecules (not shown) from the solvation layers leads to a gain in translational entropy, compensating for the loss of conformational entropy in the biomolecules.

Cell interaction

We also investigated the interaction between BK-DNA complexes and cell membranes. These assays have been performed using HEK-293t cells, a common and widely applied model for the internalization of exogenous biomolecules.^{61,62} Cytotoxicity evaluations using MTT assays revealed that both BK alone and BK-DNA complexes (2:1 charge ratio) are well-tolerated, demonstrating no significant toxicity even at high peptide concentrations of up to 3.6 mM (see SI file, Figure S9). Cells were incubated with BK-DNA complexes, and the fluorescence of YOYO-1-labeled DNA fragments was monitored to examine the fate of the complexes. In Figure 5, bottom row, confocal microscopy images reveal that cells incubated with BK-DNA display green fluorescence throughout the cytosol, a similar effect observed in previous works exploring the action of non-covalent complexes formed between CPPs and DNA.^{24,30} In contrast, cells incubated with YOYO-1-labeled DNA fragments without BK do not show significant fluorescence glow, demonstrating the inability of naked DNA to penetrate cell membranes (Figure

5B). Comparisons made with the increase in fluorescence levels of reporter DNA using complexes formed with the transfecting reagent lipofectamine indicate that the fluorescence increase in the presence of BK is approximately two-thirds lower. Therefore, although this observation acknowledges the low uptake capabilities of BK compared to a well-established transfecting reagent, it also reveals a novel feature that has not been reported for BK previously. Cell-penetrating peptides (CPPs) that share physicochemical similarities with BK, such as low molecular weight, the presence of arginine residues, and hydrophobic segments composed of prolines, have been observed to penetrate cells through various mechanisms, including the formation of transient pores and lipid rafts.⁶³⁻⁶⁵ In this context, we propose that similar routes may also be involved in the penetration of BK complexes. It is worthy note that the HEK-293t cells do not bear B2 receptors which are involved in the BK physiology. Therefore, the mechanisms underlying the penetration capabilities of this peptide are likely to be correlated with its physicochemical features rather than relying on a receptor-specific mechanism.

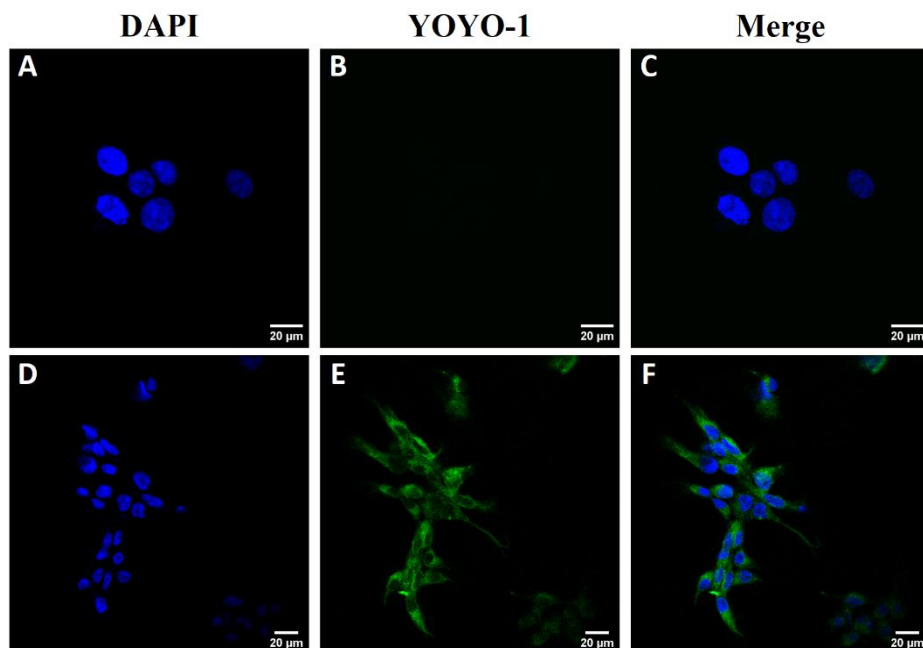


Figure 5: Fluorescence images of HEK-293t cells incubated with BK-DNA complexes. The DNA fragments (~150 bp) were labeled with YOYO-1 and are shown as greenish fluorescence. The top row shows control samples incubated with uncomplexed DNA, whereas the bottom row show cells incubated with BK-DNA. Cell nuclei are DAPI-stained for clarity.

The bioactivity of non-covalent BK-DNA complexes at modulating Ca^{2+} response in endothelial cells was also examined. For these assays, we monitored the fluorescence of a calcium-sensitive dye, Fluo-4M, as a function of time in HUVEC cell cultures to which either BK or BK-DNA complexes have been added.⁶⁶ Ca^{2+} is an important intracellular signal that regulates a variety of cell processes,⁶⁷ playing a central role in the vasodilator mechanism of BK.² Therefore, the cytoplasmatic levels of Ca^{2+} can be used as a reporter of the activity of BK-DNA. In Figure 6, the results from these kinetic measurements show that addition of BK triggers an extremely rapid elevation of Ca^{2+} concentration in the culture, with a fluorescence spike appearing immediately after addition of peptide to the culture. This almost-instantaneous signature, with such an intense variation of Ca^{2+} levels within a short time, is an indication of the strong agonistic activity of BK for B2 receptors. The process exhibits a transient feature, with fluorescence levels regularly decaying within a few minutes, indicating the consumption of Ca^{2+} .

When BK-DNA complexes are added to the cells, a similar agonistic activity is observed, with Ca^{2+} levels reaching practically the same levels observed for the native peptide. Again, the process takes place very quickly, thus indicating that agonistic activity of complexes remains at similar levels of that of the native peptide. Thus, we may conclude that complexes formed between BK and DNA likely retain affinity for the B2 receptor and are able to promote Ca^{2+} response. As a whole, the findings above suggest that non-covalent complexation with DNA is not deleterious to vasodilation properties of BK.

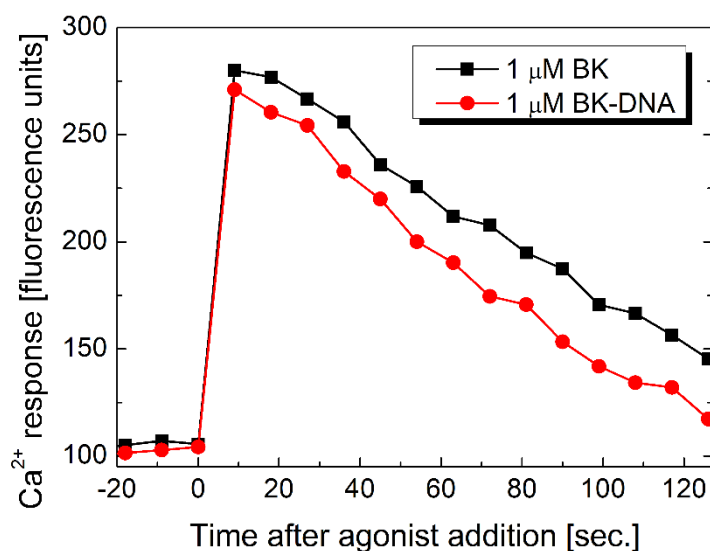


Figure 6: Fluorescence measurements of the intracellular Ca²⁺ concentration in HuVEC cells incubated with 1 μM BK (A) and BK-DNA complexes (1 μM peptide, 6:1 molar ratio). The agonist was added to the culture at $t = 0$ s.

CONCLUSIONS:

We have developed a strategy using DNA fragments as a template for driving the self-assembly of bradykinin into highly ordered, 1D structures. Our data indicate that the interaction between BK and DNA occurs primarily via minor-groove sites, suggesting that electrostatic attraction plays a significant role in the complexation process. The combination of microscopy approaches and small-angle scattering provided nanoscale information on these new structures, demonstrating that BK-DNA complexes form fibrillar assemblies, while the peptide alone lacks the ability to form regular structures in solution. Importantly, we also observed that the BK-DNA complexes are able to promote an improvement in the fluorescence of reporter DNA in HEK-293t cells, which may suggest that BK possesses some cell-penetrating peptide abilities, a feature which has not been previously reported. Therefore, our findings suggest that BK also merits further investigation for optimizing this aspect, which may be useful in the design of multifunctional materials. Our results suggest that the association with DNA does not negatively affect the modulating capabilities of the peptide, and the BK-DNA nanostructures preserve their native bioactivity, including the ability to regulate ion channels in the cell membranes of vascular cells. Thus, we propose that these highly ordered fibrillar structures have the potential to be

developed as novel therapeutics with hypotensive effects and should be a topic for future research to examine blood pressure via *in vivo* studies. In conclusion, our findings demonstrate a promising strategy for the fabrication of highly ordered, 1D structures of BK using DNA as a template, which may have applications in the development of nanotherapeutics for hypertension and related disorders.

AUTHOR CONTRIBUTIONS:

ERS and CRN designed the research. TCL performed sample preparations, fluorescence, and microscopy experiments. IWH and VC performed SAXS data collection and provided structural insights. RNB performed SAXS and TEM data analysis. LRM and MYI performed cellular assays and data analysis. The manuscript was written by TCL and ERS with inputs from all contributors. The final version was revised and approved by all authors.

CONFLICT OF INTERESTS:

There are no conflicts of interest to declare.

ACKNOWLEDGEMENTS:

This study has been primarily supported by the Sao Paulo Research Foundation, FAPESP, under grants #22/03056-6 to ERS and #21/04885-3 to CRN. The Brazilian Council for Scientific Research, CNPq, is acknowledged for grant #409455/2018-0 (to ERS) and post-doctoral fellowship #402154/2022-3 (to RNB). ERS and CRN are recipients of CNPq fellowships (#307443/2022-1 and #306174/2022-7). TCL thanks the Coordination for the Improvement of Higher Education Personnel, CAPES, for a PhD fellowship (finance code 001). LRM thanks FAPESP for PhD fellowships (#2019/19719-1 and #2021/10092-6). The Brazilian Nanotechnology National Laboratory (LNNano) is acknowledged for granting access to TEM and AFM instruments under proposals: #TEM-24500 and #20220321, and we are grateful to Dr. Carlos Costa and Dr. Antonio Borges for assistance. Prof. Sang Han (Biophysics Dept, UNIFESP) is acknowledged for providing access to culture facilities during the revision process. We thank Diamond for the award of beamtime (SM29895-1) and we thank Nikul Khunti for assistance with the experiments.

REFERENCES

- (1) Shen, J.; Zhang, H. Function and Structure of Bradykinin Receptor 2 for Drug Discovery. *Acta Pharmacol. Sin.* **2023**, *44* (3), 489–498.
- (2) Golias, C.; Charalabopoulos, A.; Stagikas, D.; Charalabopoulos, K.; Batistatou, A. The Kinin System-Bradykinin: Biological Effects and Clinical Implications. Multiple Role of the Kinin System-Bradykinin. *Hippokratia* **2007**, *11* (3), 124–128.
- (3) Rocha e Silva, M.; Beraldo, W. T.; Rosenfeld, G. Bradykinin, a Hypotensive and Smooth Muscle Stimulating Factor Released from Plasma Globulin by Snake Venoms and by Trypsin. *Am. J. Physiol.* **1949**, *156* (2), 261–273.
- (4) Huang, P. L.; Huang, Z. H.; Mashimo, H.; Bloch, K. D.; Moskowitz, M. A.; Bevan, J. A.; Fishman, M. C. Hypertension in Mice Lacking the Gene for Endothelial Nitric-Oxide Synthase. *Nature* **1995**, *377* (6546), 239–242.
- (5) Vanhoutte, P. M.; Shimokawa, H.; Feletou, M.; Tang, E. H. C. Endothelial Dysfunction and Vascular Disease - a 30th Anniversary Update. *ACTA Physiol.* **2017**, *219* (1), 22–96.
- (6) Lerner, U. H.; Modeer, T. Bradykinin-B1 and Bradykinin-B2 Receptor Agonists Synergistically Potentiate Interleukin-1-Induced Prostaglandin Biosynthesis in Human Gingival Fibroblasts. *Inflammation* **1991**, *15* (6), 427–436.
- (7) Rex, D. A. B.; Vaid, N.; Deepak, K.; Dagamajalu, S.; Prasad, T. S. K. A Comprehensive Review on Current Understanding of Bradykinin in COVID-19 and Inflammatory Diseases. *Mol. Biol. Rep.* **2022**, *49* (10), 9915–9927.
- (8) Wilczynski, S. A.; Wenceslau, C. F.; McCarthy, C. G.; Webb, R. C. A Cytokine/Bradykinin Storm Comparison: What Is the Relationship Between Hypertension and COVID-19? *Am. J. Hypertens.* **2021**, *34* (4), 304–306.
- (9) Roche, J. A.; Roche, R. A Hypothesized Role for Dysregulated Bradykinin Signaling in COVID-19 Respiratory Complications. *FASEB J.* **2020**, *34* (6), 7265–7269.
- (10) McCarthy, C. G.; Wilczynski, S.; Wenceslau, C. F.; Webb, R. C. A New Storm on the Horizon in COVID-19: Bradykinin-Induced Vascular Complications. *Vascul. Pharmacol.* **2021**, *137*, 106826.
- (11) Zhang, Y.; Lu, Y.; Wang, F.; An, S.; Zhang, Y.; Sun, T.; Zhu, J.; Jiang, C. ATP/PH Dual Responsive Nanoparticle with d-[Des-Arg¹⁰]Kallidin Mediated Efficient In Vivo Targeting Drug Delivery. *Small* **2017**, *13* (3), 1602494.
- (12) Rauschenbach, S.; Rinke, G.; Gutzler, R.; Abb, S.; Albarghash, A.; Le, D.; Rahman, T. S.; Dürr, M.; Harnau, L.; Kern, K. Two-Dimensional Folding of Polypeptides into Molecular Nanostructures at Surfaces. *ACS Nano* **2017**, *11* (3), 2420–2427.
- (13) Habibi, N.; Shafiee, H.; Kamaly, N.; Memic, A. Self-Assembled Peptide-Based Nanostructures: Smart Nanomaterials toward Targeted Drug Delivery. *Nano Today* **2016**, *11* (1).
- (14) Li, T.; Lu, X.-M.; Zhang, M.-R.; Hu, K.; Li, Z. Peptide-Based Nanomaterials: Self-Assembly, Properties and Applications. *Bioact. Mater.* **2022**, *11*, 268–282.
- (15) Rong, L.; Lei, Q.; Zhang, X.-Z. Recent Advances on Peptide-Based Theranostic Nanomaterials. *VIEW* **2020**, *1* (4), 20200050.

- (16) Hutchinson, J. A.; Burholt, S.; Hamley, I. W. Peptide Hormones and Lipopeptides: From Self-Assembly to Therapeutic Applications. *J. Pept. Sci.* **2017**, *23* (2), 82–94.
- (17) Hamley, I. W. Self-Assembly, Bioactivity, and Nanomaterials Applications of Peptide Conjugates with Bulky Aromatic Terminal Groups. *ACS Appl. Bio Mater.* **2023**, *6* (2), 384–409.
- (18) Yang, Y.; Jia, X.; Zhang, Y.-M.; Li, N.; Liu, Y. Supramolecular Nanoparticles Based on β -CD Modified Hyaluronic Acid for DNA Encapsulation and Controlled Release. *Chem. Commun.* **2018**, *54* (63), 8713–8716.
- (19) Li, F.-Q.; Yu, Q.-L.; Liu, Y.-H.; Yu, H.-J.; Chen, Y.; Liu, Y. Highly Efficient Photocontrolled Targeted Delivery of siRNA by a Cyclodextrin-Based Supramolecular Nanoassembly. *Chem. Commun.* **2020**, *56* (27), 3907–3910.
- (20) Hu, P.; Chen, Y.; Liu, Y. Cyclodextrin-Based Switchable DNA Condenser. *Chem. Commun.* **2015**, *51* (54), 10839–10842.
- (21) Palmer, L. C.; Stupp, S. I. Molecular Self-Assembly into One-Dimensional Nanostructures. *Acc Chem Res* **2008**, *41* (12), 1674–1684.
- (22) Beniash, E.; Hartgerink, J. D.; Storrie, H.; Stendahl, J. C.; Stupp, S. I. Self-Assembling Peptide Amphiphile Nanofiber Matrices for Cell Entrapment. *Acta Biomater* **2005**, *1* (4), 387–397.
- (23) Li, H.; Park, S. H.; Reif, J. H.; LaBean, T. H.; Yan, H. DNA-Templated Self-Assembly of Protein and Nanoparticle Linear Arrays. *J. Am. Chem. Soc.* **2004**, *126* (2), 418–419.
- (24) Mello, L. R.; Hamley, I. W.; Castelletto, V.; Garcia, B. B. M.; Lourenço, T. C.; Vassiliades, S. V.; Alves, W. A.; Han, S. W.; Silva, E. R. Self-Assembly and Intracellular Delivery of DNA by a Truncated Fragment Derived from the Trojan Peptide Penetratin. *Soft Matter* **2020**, *16* (20), 4746–4755.
- (25) Ruff, Y.; Moyer, T.; Newcomb, C. J.; Demeler, B.; Stupp, S. I. Precision Templating with DNA of a Virus-like Particle with Peptide Nanostructures. *J. Am. Chem. Soc.* **2013**, *135* (16), 6211–6219.
- (26) Mello, L. R.; Aguiar, R. B.; Yamada, R. Y.; Moraes, J. Z.; Hamley, I. W.; Alves, W. A.; Reza, M.; Ruokolainen, J.; Silva, E. R. Amphiphathic Design Dictates Self-Assembly, Cytotoxicity and Cell Uptake of Arginine-Rich Surfactant-like Peptides. *J. Mater. Chem. B* **2020**, *8* (12), 2495–2507.
- (27) De Mello, L. R.; Hamley, I. W.; Castelletto, V.; Garcia, B. B. M.; Han, S. W.; De Oliveira, C. L. P.; Da Silva, E. R. Nanoscopic Structure of Complexes Formed between DNA and the Cell-Penetrating Peptide Penetratin. *J. Phys. Chem. B* **2019**, *123* (42), 8861–8871.
- (28) Coledam, D. A. C.; Pupo, M. M. S.; Silva, B. F.; Silva, A. J.; Eguiluz, K. I. B.; Salazar-Banda, G. R.; Aquino, J. M. Electrochemical Mineralization of Cephalexin Using a Conductive Diamond Anode: A Mechanistic and Toxicity Investigation. *Chemosphere* **2017**, *168*, 638–647.
- (29) Rehman, S. U.; Yaseen, Z.; Husain, M. A.; Sarwar, T.; Ishqi, H. M.; Tabish, M. Interaction of 6 Mercaptopurine with Calf Thymus DNA – Deciphering the Binding Mode and Photoinduced DNA Damage. *PLoS One* **2014**, *9* (4), 1–11.
- (30) de Mello, L. R.; Porosk, L.; Lourenço, T. C.; Garcia, B. B. M.; Costa, C. A. R.; Han, S. W.; de Souza, J. S.; Langel, Ü.; da Silva, E. R. Amyloid-like Self-Assembly of a Hydrophobic Cell-Penetrating Peptide and Its Use as a Carrier for Nucleic Acids. *ACS Appl. Bio Mater.* **2021**, *4* (8), 6404–6416.

- (31) da Silva, E. R. T.; de Oliveira, E. A.; Fevrier, A.; Nallet, F.; Navailles, L. Supramolecular Polymorphism of DNA in Non-Cationic L-Alpha Lipid Phases. *Eur Phys J E Soft Matter* **2011**, *34* (8), 83.
- (32) Souza, B. B. S.; Lourenço, T. C.; Gerbelli, B. B.; Oseliero Filho, P. L.; Oliveira, C. L. P.; Miranda, A.; da Silva, E. R. A Biophysical Study of DNA Condensation Mediated by Histones and Protamines. *J. Mol. Liq.* **2022**, *368*, 120745.
- (33) Lourenço, T. C.; Mello, L. R.; Silva, B. B. S.; Silva, E. R. Molecular Structure and Supramolecular Assembly of a TGF-B1 Mimetic Oligopeptide. *J. Mol. Struct.* **2020**, *1219*, 128691.
- (34) Schneider, C. A.; Rasband, W. S.; Eliceiri, K. W. NIH Image to ImageJ: 25 Years of Image Analysis. *Nat Meth* **2012**, *9* (7), 671–675.
- (35) Necas, D.; Klapetek, P. Gwyddion: An Open-Source Software for SPM Data Analysis. *Cent. Eur. J. Phys.* **2012**, *10* (1), 181–188.
- (36) Bressler, I.; Kohlbrecher, J.; Thunemann, A. F. SASfit: A Tool for Small-Angle Scattering Data Analysis Using a Library of Analytical Expressions. *J. Appl. Crystallogr.* **2015**, *48* (5), 1587–1598.
- (37) Hawe, A.; Sutter, M.; Jiskoot, W. Extrinsic Fluorescent Dyes as Tools for Protein Characterization. *Pharm. Res.* **2008**, *25* (7), 1487–1499.
- (38) Vardevanyan, P. O.; Antonyan, A. P.; Parsadanyan, M. A.; Davtyan, H. G.; Karapetyan, A. T. The Binding of Ethidium Bromide with DNA: Interaction with Single- and Double-Stranded Structures. *Exp. Mol. Med.* **2003**, *35* (6), 527–533.
- (39) Dragan, A. I.; Pavlovic, R.; McGivney, J. B.; Casas-Finet, J. R.; Bishop, E. S.; Strouse, R. J.; Schenerman, M. A.; Geddes, C. D. SYBR Green I: Fluorescence Properties and Interaction with DNA. *J. Fluoresc.* **2012**, *22* (4), 1189–1199.
- (40) Gelbart, W. M.; Bruinsma, R. F.; Pincus, P. A.; Parsegian, V. A. DNA-Inspired Electrostatics. *Phys. Today* **2000**, *53* (9), 38–44.
- (41) Sugawara, A.; Shimada, H.; Otsubo, Y.; Kouketsu, T.; Suzuki, S.; Yokoyama, A. The Usefulness of Angiotensin-(1-7) and Des-Arg9-Bradykinin as Novel Biomarkers for Metabolic Syndrome. *Hypertens. Res.* **2021**, *44* (8), 1034–1036.
- (42) Kim, S. K.; Nordén, B. Methyl Green: A DNA Major-Groove Binding Drug. *FEBS Lett.* **1993**, *315* (1), 61–64.
- (43) Nguyen, B.; Neidle, S.; Wilson, W. D. A Role for Water Molecules in DNA-Ligand Minor Groove Recognition. *Acc. Chem. Res.* **2009**, *42* (1), 11–21.
- (44) Mertens, H. D.; Svergun, D. I. Structural Characterization of Proteins and Complexes Using Small-Angle X-Ray Solution Scattering. *J Struct Biol* **2010**, *172* (1), 128–141.
- (45) Hamley, I. W. *Small-Angle Scattering: Theory, Instrumentation, Data and Applications*, 1st ed.; Wiley: Chichester, 2021.
- (46) Silva, E. R.; Listik, E.; Han, S. W.; Alves, W. A.; Soares, B. M.; Reza, M.; Ruokolainen, J.; Hamley, I. W. Sequence Length Dependence in Arginine/Phenylalanine Oligopeptides: Implications for Self-Assembly and Cytotoxicity. *Biophys. Chem.* **2018**, *233*, 1–12.
- (47) Pedersen, J. S. Analysis of Small-Angle Scattering Data from Colloids and Polymer Solutions: Modeling and Least-Squares Fitting. *Adv. Colloid Interface Sci.* **1997**, *70* (0), 171–210.

- (48) Teixeira, J. Small-Angle Scattering by Fractal Systems. *J. Appl. Crystallogr.* **1988**, *21*, 781–785.
- (49) Hammouda, B. Clustering in Polar Media. *J. Chem. Phys.* **2010**, *133* (8), 84901.
- (50) de Mello, L. R.; Carrascosa, V.; Rebelato, E.; Juliano, M. A.; Hamley, I. W.; Castelletto, V.; Vassiliades, S. V.; Alves, W. A.; Nakaie, C. R.; da Silva, E. R. Nanostructure Formation and Cell Spheroid Morphogenesis of a Peptide Supramolecular Hydrogel. *Langmuir* **2022**, *38* (11), 3434–3445.
- (51) Rha, A. K.; Das, D.; Taran, O.; Ke, Y.; Mehta, A. K.; Lynn, D. G. Electrostatic Complementarity Drives Amyloid/Nucleic Acid Co-Assembly. *Angew. Chem. Int. Ed. Engl.* **2020**, *59* (1), 358–363.
- (52) Nilsson, M. R. Techniques to Study Amyloid Fibril Formation in Vitro. *Methods* **2004**, *34* (1), 151–160.
- (53) Manning, G. S. The Persistence Length of DNA Is Reached from the Persistence Length of Its Null Isomer through an Internal Electrostatic Stretching Force. *Biophys. J.* **2006**, *91* (10), 3607–3616.
- (54) Wagner, K.; Harries, D.; May, S.; Kahl, V.; Radler, J. O.; Ben-Shaul, A. Direct Evidence for Counterion Release upon Cationic Lipid-DNA Condensation. *Langmuir* **2000**, *16* (2), 303–306.
- (55) Achazi, K.; Haag, R.; Ballauff, M.; Dervede, J.; Kizhakkedathu, J. N.; Maysinger, D.; Multhaupt, G. Understanding the Interaction of Polyelectrolyte Architectures with Proteins and Biosystems. *Angew. Chemie Int. Ed.* **2021**, *60* (8), 3882–3904.
- (56) Yuan, C.; Levin, A.; Chen, W.; Xing, R.; Zou, Q.; Herling, T. W.; Challa, P. K.; Knowles, T. P. J.; Yan, X. Nucleation and Growth of Amino Acid and Peptide Supramolecular Polymers through Liquid–Liquid Phase Separation. *Angew. Chemie Int. Ed.* **2019**, *58* (50), 18116–18123.
- (57) Hamley, I. W. Peptide Fibrillization. *Angew Chem Int Ed Engl* **2007**, *46* (43), 8128–8147.
- (58) Zhou, P.; Xing, R.; Li, Q.; Li, J.; Yuan, C.; Yan, X. Steering Phase-Separated Droplets to Control Fibrillar Network Evolution of Supramolecular Peptide Hydrogels. *Matter* **2023**.
- (59) Yuan, C.; Ji, W.; Xing, R.; Li, J.; Gazit, E.; Yan, X. Hierarchically Oriented Organization in Supramolecular Peptide Crystals. *Nat. Rev. Chem.* **2019**, *3* (10), 567–588.
- (60) Harries, D.; May, S.; Ben-Shaul, A. Counterion Release in Membrane-Biopolymer Interactions. *Soft Matter* **2013**, *9* (39), 9268–9284.
- (61) Schmidt, S.; Adjobo-Hermans, M. J. W.; Kohze, R.; Enderle, T.; Brock, R.; Milletti, F. Identification of Short Hydrophobic Cell-Penetrating Peptides for Cytosolic Peptide Delivery by Rational Design. *Bioconjug. Chem.* **2017**, *28* (2), 382–389.
- (62) Bollin, F.; Dechavanne, V.; Chevalet, L. Design of Experiment in CHO and HEK Transient Transfection Condition Optimization. *Protein Expr. Purif.* **2011**, *78* (1), 61–68.
- (63) Bechara, C.; Sagan, S. Cell-Penetrating Peptides: 20 Years Later, Where Do We Stand? *Febs Lett.* **2013**, *587* (12), 1693–1702.
- (64) Pujals, S.; Giralt, E. Proline-Rich, Amphipathic Cell-Penetrating Peptides. *Adv. Drug Deliv. Rev.* **2008**, *60* (4–5), 473–484.

- (65) Kauffman, W. B.; Fuselier, T.; He, J.; Wimley, W. C. Mechanism Matters: A Taxonomy of Cell Penetrating Peptides. *Trends Biochem. Sci.* **2015**, *40* (12), 749–764.
- (66) Price, K. L.; Lummis, S. C. R. FlexStation Examination of 5-HT₃ Receptor Function Using Ca²⁺ - and Membrane Potential-Sensitive Dyes: Advantages and Potential Problems. *J. Neurosci. Methods* **2005**, *149* (2), 172–177.
- (67) Charlton, S. J.; Vauquelin, G. Elusive Equilibrium: The Challenge of Interpreting Receptor Pharmacology Using Calcium Assays. *Br. J. Pharmacol.* **2010**, *161* (6), 1250–1265.

ToC graphic

